

Cite this: *Chem. Sci.*, 2019, **10**, 3080

All publication charges for this article have been paid for by the Royal Society of Chemistry

Received 3rd October 2018
Accepted 16th January 2019DOI: 10.1039/c8sc04389b
rsc.li/chemical-science

CO₂ capture by Mn(**i**) and Re(**i**) complexes with a deprotonated triethanolamine ligand†

Hiroki Koizumi,^a Hiroyuki Chiba,^a Ayumi Sugihara,^b Munetaka Iwamura,^b Koichi Nozaki^{*b} and Osamu Ishitani^{ID, *a}

CO₂ capture at low concentration by catalysts is potentially useful for developing photocatalytic and electrocatalytic CO₂ reduction systems. We investigated the CO₂-capturing abilities of two complexes, *fac*-Mn(X₂bpy)(CO)₃(OCH₂CH₂NR₂) and *fac*-Re(X₂bpy)(CO)₃(OCH₂CH₂NR₂) (X₂bpy = 4,4'-X₂-2,2-bipyridine and R = -CH₂CH₂OH), which work as efficient catalysts for CO₂ reduction. Both complexes could efficiently capture CO₂ even from Ar gas containing only low concentration of CO₂ such as 1% to be converted into *fac*-M(X₂bpy)(CO)₃(OC(O)OCH₂CH₂NR₂) (M = Mn and Re). These CO₂-capturing reactions proceeded reversibly and their equilibrium constants were >1000. The substituents of X₂bpy strongly affected the CO₂-capturing abilities of both Mn and Re complexes. The density functional theory (DFT) calculation could be used to estimate the CO₂-capturing abilities of the metal complexes in the presence of triethanolamine.

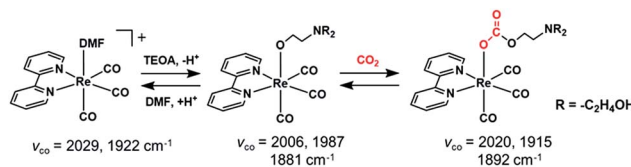
Introduction

The catalytic conversion of CO₂ into useful carbon resources by using sustainable energy such as sun light has attracted much attention as one of the technologies that address the issues of both global warming and the shortage of carbon-based resources. Transition metal complexes with ions such as Re(**i**),¹ Mn(**i**),² Ru(**i**),³ Ir(**iii**),⁴ Ni(**ii**),^{5,6} Fe(**ii**),⁷⁻¹¹ and Co(**ii**)^{12,13} have been reported as catalysts for reducing CO₂ to CO, formic acid, and/or methane. For example, *fac*-[Re(N⁺N)(CO)₃(L)]⁺ (N⁺N = diimine ligand and L = monodentate ligand) catalyses the selective conversion of CO₂ into CO in a *N,N*-dimethylformamide (DMF) solution containing triethanolamine (TEOA) *via* photocatalytic reaction or a DMF solution containing H₂O *via* electrocatalytic reaction.^{1,14} *fac*-Mn(N⁺N)(CO)₃Br has also been reported as an efficient CO₂ reduction catalyst selectively giving CO or formic acid in electrocatalytic and photocatalytic systems, respectively.^{2,15-17}

We recently found that *fac*-Re(bpy)(CO)₃(OCH₂CH₂NR₂) (**2Re-bpy**: bpy = 2,2'-bipyridine and R = -CH₂CH₂OH), which has a deprotonated triethanolamine ligand, can capture a CO₂ molecule even at low concentration of CO₂ by CO₂ insertion into the Re(**i**)-oxygen bond (Scheme 1).¹⁸ Since this CO₂ insertion is a reversible reaction with a large equilibrium constant, more than 93% of the Re complex is converted into a CO₂ adduct, *i.e.*,

fac-Re(bpy)(CO)₃(OC(O)OCH₂CH₂NR₂) (**4Re-bpy**), when bubbled with Ar gas containing only 10% CO₂ (1.6 × 10⁻² M in solution). This CO₂ capture reaction by the Re(**i**) complex was successfully applied to photocatalytic CO₂ reduction at low concentration of CO₂.¹⁹ A Ru(**ii**)-Re(**i**) photocatalyst consisting of a Ru photosensitiser unit and *fac*-Re(BL)(CO)₃(OCH₂CH₂NR₂) (BL = bridging ligand) as a catalyst unit shows almost same the photocatalytic efficiency and selectivity for CO₂ reduction in an atmosphere of 10% CO₂ as that in a 100% CO₂ (0.13 M in solution) atmosphere. Even at 0.5% CO₂ concentration, its photocatalytic efficiency was about 60% of that at 100% CO₂ concentration. These results suggest that the ability of metal complex catalysts to capture CO₂ using the deprotonated TEOA ligand potentially offers an effective method for reducing low-concentration CO₂ atmospheres without the need for condensation.

Although some similar CO₂ insertion reactions into the M-OR bond of other alkoxide metal complexes, such as M = Mn(**i**)^{20,21} and Re(**i**)^{22,23} and R = -CH₃ and -C₂H₅, have been reported,²⁴⁻⁴⁶ systematic and quantitative research, especially into the effects of different ligands and/or different central metal ions on the CO₂ capture reactions, has not yet been reported to the best of our knowledge.



Scheme 1 Ligand substitution and CO₂ capture reactions of the Re(**i**) complex and the ν_{CO} values of the Re complexes.

^aDepartment of Chemistry, School of Science, Tokyo Institute of Technology, 2-12-1, NE-1 O-okayama, Meguro-ku, Tokyo 152-8550, Japan. E-mail: ishitani@chem.titech.ac.jp

^bGraduate School of Science and Engineering, University of Toyama, 3190 Gofuku, Toyama 930-8555, Japan

† Electronic supplementary information (ESI) available. See DOI: 10.1039/c8sc04389b



Here we report the CO_2 capture abilities of $\text{Mn}(\text{i})$ 4,4'-X₂bpy tricarbonyl complexes, where X is any substituent of the corresponding $\text{Re}(\text{i})$ complexes, *i.e.*, X = H, Br, and MeO; *fac*- $[\text{Mn}(\text{X}_2\text{bpy})(\text{CO})_3(\text{OCH}_2\text{CH}_2\text{NR}_2)]$ efficiently captured CO_2 in the same manner as the $\text{Re}(\text{i})$ complexes but the corresponding $\text{W}(\text{0})$ bpy tricarbonyl complex did not. The abilities of the $\text{Mn}(\text{i})$ complexes to capture CO_2 were different from those of the corresponding $\text{Re}(\text{i})$ complexes and the abilities of both the $\text{Mn}(\text{i})$ and $\text{Re}(\text{i})$ complexes were strongly dependent on the substituents on the diimine ligand. We successfully clarified the reasons for these dependences of the CO_2 capture abilities by using density functional theory (DFT) calculations.

Results and discussion

Ligand substitution of *fac*- $[\text{M}(\text{X}_2\text{bpy})(\text{CO})_3(\text{MeCN})]^{+}$ in a DMF-TEOA mixed solution

As a typical example, *fac*- $[\text{Mn}(\text{bpy})(\text{CO})_3(\text{MeCN})]^{+}$ (5.0 mM) was added to an Ar-saturated DMF solution containing TEOA (1.3 M), and the changes in the vibrational bands of the CO ligands (ν_{CO}) were followed by FT-IR. In Fig. 1, the peaks at $\nu_{\text{CO}} = 2046$ and 1970 cm^{-1} were attributed to the starting complex and their intensity gradually decreased and new absorption bands appeared over time. After 30 min, there were no more changes in the IR spectrum and the main bands were observed at $\nu_{\text{CO}} = 2040$, 1943, and 1936 cm^{-1} , which are attributed to *fac*- $[\text{Mn}(\text{bpy})(\text{CO})_3(\text{DMF})]^{+}$ (**1Mn-bpy**) based on the similarity of the highest wavenumber peaks to those of the starting complex in the case of the $\text{Re}(\text{i})$ complex.

Some shoulder peaks were also observed at $\nu_{\text{CO}} = 2020$ and 1900 cm^{-1} . Fig. 2a shows the IR spectra measured several hours after dissolving the same complex into DMF solutions containing different concentrations of TEOA. At higher concentration of TEOA, the intensity of the peaks at $\nu_{\text{CO}} = 2020$ and 1900 cm^{-1} increased. We focussed on the totally symmetric vibrational bands around 2050 – 2010 cm^{-1} for understanding how many complexes were produced in the DMF-TEOA mixed solution. We could not reasonably fit these spectra by using curve-fitting with two components, but by using three components, we were able to identify three bands at $\nu_{\text{CO}} = 2040$, 2030, and 2017 cm^{-1} (Fig. S1†). The peak at $\nu_{\text{CO}} = 2040 \text{ cm}^{-1}$ was attributed to **1Mn-bpy**. The peak at $\nu_{\text{CO}} = 2017 \text{ cm}^{-1}$ can be attributed to *fac*- $[\text{Mn}(\text{bpy})(\text{CO})_3(\text{OCH}_2\text{CH}_2\text{NR}_2)]$ (**2Mn-bpy**) because it became larger with increased TEOA concentration

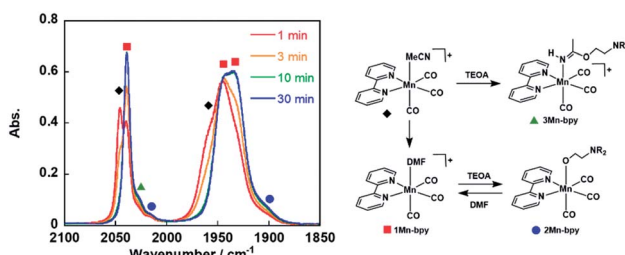


Fig. 1 Changes in the IR spectra of *fac*- $[\text{Mn}(\text{bpy})(\text{CO})_3(\text{MeCN})]^{+}$ (◆, 5.0 mM) in a DMF solution containing TEOA (1.3 M) under an Ar atmosphere over 30 min: ■, **1**-Mnbpy; ●, **2**-Mnbpy; ▲, **3**-Mnbpy.

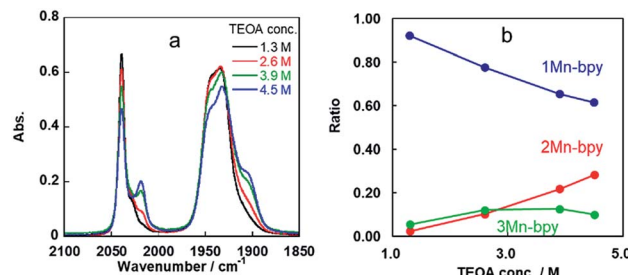


Fig. 2 (a) IR spectra of *fac*- $[\text{Mn}(\text{bpy})(\text{CO})_3(\text{MeCN})]^{+}$ in DMF solutions containing different concentrations of TEOA (1.3 M, black line; 2.6 M, red line; 3.9 M, green line; 4.5 M, blue line). (b) Ratios of **1Mn-bpy** (blue), **2Mn-bpy** (red) and **3Mn-bpy** (green) obtained by curve-fitting of the IR spectra between 2000 and 2060 cm^{-1} (Fig. S1†).

(Fig. 2a). The difference in the IR bands of **2Mn-bpy** and **1Mn-bpy** ($\Delta\nu = 22 \text{ cm}^{-1}$) was very similar to the difference between *fac*- $[\text{Re}(\text{bpy})(\text{CO})_3(\text{OCH}_2\text{CH}_2\text{NR}_2)]$ and *fac*- $[\text{Re}(\text{bpy})(\text{CO})_3(\text{DMF})]^{+}$ ($\Delta\nu = 23 \text{ cm}^{-1}$, Scheme 1). This kind of shift to a lower energy of ν_{CO} could be caused by an increase in π back donation from the Mn centre to the CO ligand because of the anionic alkoxide ligand instead of the neutral DMF. Fig. 2b shows the relationship between the peak area ratio of these complexes and the concentration of TEOA. The ratio of **1Mn-bpy** decreased with increasing TEOA concentration; however, **2Mn-bpy** showed a reverse correlation. From these results, it was concluded that **1Mn-bpy** and **2Mn-bpy** should be in equilibrium with each other in DMF-TEOA. On the other hand, the small peak at $\nu_{\text{CO}} = 2030 \text{ cm}^{-1}$ did not strongly depend on the TEOA concentration. This was probably due to a Mn(i) complex with an imidate ester ligand, *i.e.*, *fac*- $[\text{Mn}(\text{bpy})(\text{CO})_3(-\text{NH}=\text{C}(\text{CH}_3)-\text{OCH}_2\text{CH}_2\text{NR}_2)]^{+}$ (**3Mn-bpy**), which is produced by the addition of deprotonated TEOA to the MeCN ligand (Fig. 1, right scheme). The difference in the totally symmetric vibrational band from *fac*- $[\text{Mn}(\text{bpy})(\text{CO})_3(\text{MeCN})]^{+}$ was $\Delta\nu_{\text{CO}} = 16 \text{ cm}^{-1}$, and a similar peak shift was observed when *fac*- $[\text{Mn}(\text{bpy})(\text{CO})_3(\text{MeCN})]^{+}$ was dissolved in a MeCN-TEOA (5 : 1, v/v) solution ($\Delta\nu_{\text{CO}} = 14 \text{ cm}^{-1}$, Fig. S2†). This identification is also supported by the fact that the difference in ν_{CO} between *fac*- $[\text{Re}(\text{bpy})(\text{CO})_3(\text{MeCN})]^{+}$ and *fac*- $[\text{Re}(\text{bpy})(\text{CO})_3(-\text{NH}=\text{C}(\text{CH}_3)-\text{OCH}_2\text{CH}_2\text{NR}_2)]^{+}$ was $\Delta\nu_{\text{CO}} = 13 \text{ cm}^{-1}$. This reaction was much slower in the case of the Mn(i) complex than that of the corresponding Re(i) complex. To further clarify the identity of this minor product, the following experiment was performed. *fac*- $[\text{Mn}(\text{bpy})(\text{CO})_3(\text{MeCN})]^{+}$ was dissolved in a DMF solution containing 1.3 M TEOA. After 60 min, additional TEOA or DMF was added to this solution, *i.e.*, the concentration of TEOA in the solution was changed from 1.3 to 3.9 or 0.65 M. The changes in the concentration of the solvent did not affect the concentration of the minor product in either case (Fig. S2†). This suggests that the minor product was **3Mn-bpy**, which was only produced by the reaction between *fac*- $[\text{Mn}(\text{bpy})(\text{CO})_3(\text{MeCN})]^{+}$ and TEOA, was stable in the solution. In other words, the presence of **3Mn-bpy** in the solution should not affect the equilibrium between **1Mn-bpy** and **2Mn-bpy**. Therefore, in the following discussion, we consider only the equilibrium between the DMF and TEOA complexes.

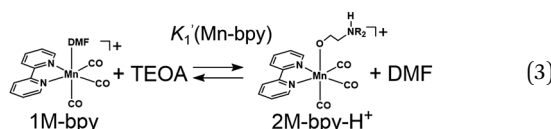


There are two possible equilibrium equations (eqn (1) and (3)) for the conversion of **1Mn-bpy** into **2Mn-bpy**. In the mechanism described in eqn (3), one TEOA molecule works as both a nucleophile and a base. In the case of eqn (1), two TEOA molecules contribute to the ligand substitution reaction, where proton capture from the TEOA interacting with the metal centre by the other TEOA molecule is considered. In this ligand substitution, the main mechanism is probably described in eqn (1) because the solution contained a very high concentration of TEOA (>1.3 M). Therefore, we chose eqn (1) for the DFT calculation as described below.[‡]

In eqn (2), the concentration of the protonated TEOA ($[\text{H-TEOA}^+]$) was assumed to be the same as that of **2Mn-bpy** because the proton that originated in the TEOA ligand should be captured by another TEOA molecule as described above. The concentrations of the Mn(i) complexes were calculated by curve-fitting of the IR spectra and were used to determine the equilibrium constant, *i.e.*, $K_1(\text{Mn-bpy}) = (0.22 \pm 0.03) \times 10^{-3}$, by using eqn (2).



$$K_1(\text{Mn-bpy}) = \frac{[2\text{M-bpy}][\text{DMF}][\text{H-TEOA}^+]}{[1\text{M-X}_2\text{bpy}][\text{TEOA}]^2} \approx \frac{[2\text{M-bpy}]^2[\text{DMF}]}{[1\text{M-X}_2\text{bpy}][\text{TEOA}]^2} \quad (2)$$



When the Mn complexes with substituents at the 4,4'-position of the bpy ligand, *i.e.*, $\text{fac-}[\text{Mn}(\text{X}_2\text{bpy})(\text{CO})_3(\text{MeCN})]^+$ ($\text{X} = \text{Br}$ and OMe), were dissolved in the DMF-TEOA mixed solution, similar IR spectral changes were observed in both cases (Fig. S4†). However, the equilibrium constants were very different from $K_1(\text{Mn-bpy})$. Electron-withdrawing substituents gave a larger constant, *i.e.*, $K_1(\text{Mn-Br}_2\text{bpy}) = (0.64 \pm 0.03) \times 10^{-3}$. On the other hand, electron-donating substituents gave a smaller constant, *i.e.*, $K_1(\text{Mn-(MeO)}_2\text{bpy}) = (0.12 \pm 0.01) \times 10^{-3}$. These results strongly suggest that stronger electron-withdrawing substituents on the X_2bpy ligand give rise to higher stability of **2-Mn-X₂bpy**.

In the case of the corresponding Re(i) complex, $\text{fac-}[\text{Re}(\text{X}_2\text{bpy})(\text{CO})_3(\text{MeCN})]^+$ was converted into $\text{fac-}[\text{Re}(\text{X}_2\text{bpy})(\text{CO})_3(\text{DMF})]^+$ (**1Re-X₂bpy**) by first dissolving in DMF § and then into $\text{fac-}[\text{Re}(\text{X}_2\text{bpy})(\text{CO})_3(\text{OCH}_2\text{CH}_2\text{NR}_2)]^+$ (**2Re-X₂bpy**) by the addition of TEOA to the solution because this procedure could suppress the formation of $[\text{Re}(\text{bpy})(\text{CO})_3(-\text{NH}=\text{C}(\text{CH}_3)-\text{OCH}_2\text{CH}_2\text{NR}_2)]^+$ (**3Re-bpy**).¹⁸ ¶ The equilibrium constants between **1Re-X₂bpy** and **2Re-X₂bpy** are summarised in Table 2. The values of $K_1(\text{Re-X}_2\text{bpy})$

are consistent with those of the corresponding Mn complexes as described above, *i.e.*, the electron-withdrawing substituents on the X_2bpy ligand yielded a larger equilibrium constant. The equilibrium constant of the Re complexes was much larger than that of the corresponding Mn complexes, for example, $K_1(\text{Re-bpy}) = (71 \pm 1) \times 10^{-3}$ and $K_1(\text{Mn-bpy}) = (0.64 \pm 0.03) \times 10^{-3}$, that is, the formation of **2Mn-X₂bpy** was thermodynamically less favourable compared to that of the corresponding Re(i) complex in the DMF-TEOA mixed solution.

CO₂ capture by *fac*-M(X_2bpy)(CO)₃(OCH₂CH₂NR₂)

Introduction of CO₂ into the DMF-TEOA solution containing the equilibrium mixture of **1Mn-bpy** and **2Mn-bpy** caused rapid disappearance of the ν_{CO} bands attributed to **1Mn-bpy** and **2Mn-bpy** and the appearance of three new ν_{CO} bands at 2028, 1936, and 1913 cm⁻¹ (Fig. 3a). When this CO₂-saturated solution was bubbled with Ar for 30 min, the original ν_{CO} bands of **1Mn-bpy** and **2Mn-bpy** were fully recovered (Fig. S5†). These IR spectral changes are very similar to those of the corresponding Re(i) complexes, where both **1Re-bpy** and **2Re-bpy** were converted into the CO₂ adduct complex *fac*-Re(bpy)(CO)₃(OC(O)OCH₂CH₂NR₂) (**4Re-bpy**) upon bubbling with CO₂.¹⁸ These results strongly suggest that CO₂ capture by the Mn(i) complex proceeded well and that the reaction was reversible. Identification of the CO₂ adduct was confirmed by ¹H and ¹³C NMR experiments in a DMSO-*d*₆ solution containing TEOA.

DMF-*d*₇ was not used because the signal of a carbonate carbon (M-OC(O)O-R) is expected to be observed at a similar magnetic field to that of the amide carbon of DMF. We confirmed that even in a DMSO-TEOA mixed solution, similar IR spectral changes occurred to those in the DMF-TEOA solution (Fig. 3b). The ¹H NMR spectra of the solution containing the Mn complexes were first measured under an Ar atmosphere and then measured again after bubbling with CO₂ for 3 min (Fig. S6†). The ¹H NMR signals attributed to the bpy ligands changed completely before and after bubbling with CO₂; the proton peaks attributed to the bpy ligands of **1Mn-bpy** and **2Mn-bpy**, which were observed under an Ar atmosphere, disappeared and four new proton signals were observed at a higher magnetic field under a CO₂ atmosphere. Fig. 4a shows the ¹³C NMR spectrum with proton decoupling; a singlet peak attributable to the carbonate carbon (M-OC(O)O-R) at 158.7 ppm was observed under the CO₂ atmosphere. This signal was drastically enhanced by using ¹³CO₂ (99% ¹³C content)

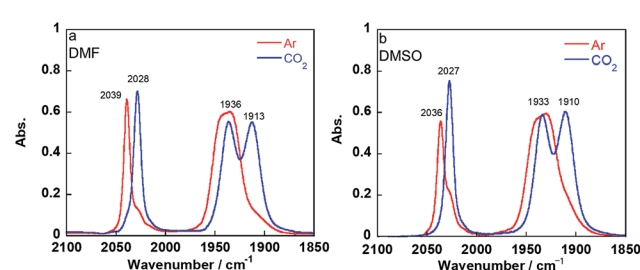


Fig. 3 IR spectra of the equilibrated mixture of **1Mn-bpy** and **2Mn-bpy** in DMF (a) or DMSO (b) containing TEOA (1.3 M) after Ar bubbling (red line) and CO₂ bubbling (blue line) for 15 min.



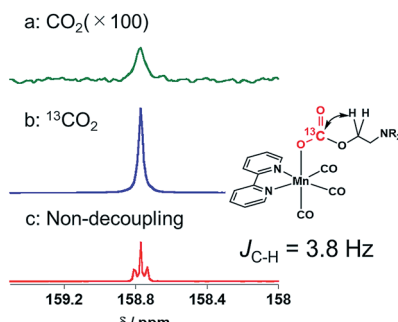
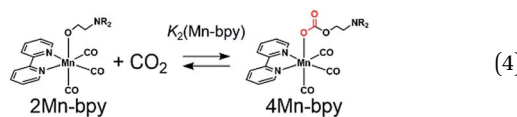


Fig. 4 ^{13}C NMR spectra of a DMSO- d_6 solution containing TEOA (1.3 M) and the Mn complexes (1Mn-bpy and 2Mn-bpy; their total concentration was 35 mM) after bubbling with (a) CO_2 and (b) $^{13}\text{CO}_2$; both are proton-decoupled. (c) The spectrum without proton decoupling for the same sample as in (b).

instead of CO_2 (Fig. 4b). Without proton decoupling, the signal at 158.7 ppm became a triplet with $J_{\text{C-H}} = 3.8 \text{ Hz}$ (Fig. 4c). This is attributable to long-range coupling with the methylene group in the deprotonated TEOA moiety of the carbonate ester ligand (Fig. 4) because a similar signal was reported in the ^{13}C NMR spectrum of 3Re-bpy (158.4 ppm, 3.6 Hz).¹⁸ These results strongly suggest that the insertion reaction of CO_2 into the Mn–O bond in 2Mn-bpy gives the complex $\text{fac-}[\text{Mn}(\text{bpy})(\text{CO})_3(\text{OC(O)OCH}_2\text{CH}_2\text{NR}_2)]$ (4Mn-bpy) (eqn (5)).

As shown in Fig. 5a, the ratios of the peaks changed with the CO_2 concentration in the solution. We successfully conducted curve-fitting to obtain the concentrations of 1Mn-bpy, 2Mn-bpy and 4Mn-bpy as shown in Fig. 5b. Direct determination of $K_2(\text{Mn-bpy})$ from the peak area of 2Mn-bpy showed a large experimental error because the peak of 2Mn-bpy was very small. Therefore, $K_2(\text{Mn-bpy})$ was calculated by using eqn (7) with $K_1(\text{Mn-bpy})$ and $K_3(\text{Mn-bpy})$, which is the equilibrium constant between 1Mn-bpy and 4Mn-bpy (eqn (6) and (7)). In eqn (7), the concentration of the protonated TEOA ($[\text{H-TEOA}^+]$) was assumed to be the same as the total concentrations of 2Mn-bpy and 4Mn-bpy because of the same reason in the case of eqn (2). This calculation method gave much lower experimental error; the value of $K_2(\text{Mn-bpy})$ between 2Mn-bpy and 4Mn-bpy was obtained to be $(61 \pm 12) \times 10^3 \text{ M}^{-1}$.



$$K_2(\text{Mn-bpy}) = \frac{[\text{4Mn-bpy}]}{[\text{2Mn-bpy}][\text{CO}_2]} \quad (5)$$

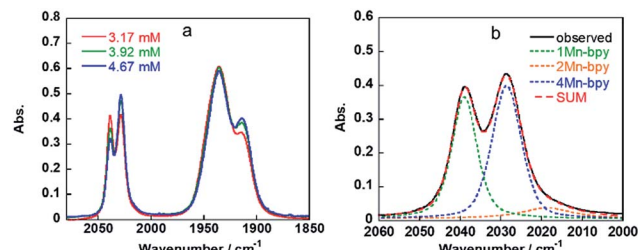
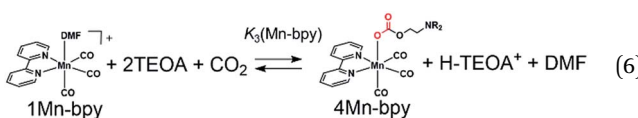


Fig. 5 IR spectra of $\text{fac-}[\text{Mn}(\text{bpy})(\text{CO})_3(\text{MeCN})]^+$ in DMF containing 1.3 M TEOA and different concentrations of CO_2 (a) and the curve-fitting result for the observed spectra at 3.17 mM CO_2 (b).

$$\begin{aligned} K_3(\text{Mn}_2\text{bpy}) &= K_1(\text{Mn-bpy}) K_2(\text{Mn-bpy}) = \frac{[4\text{Mn-bpy}][\text{H-TEOA}^+][\text{DMF}]}{[1\text{Mn-bpy}][\text{TEOA}]^2[\text{CO}_2]} \\ &\approx \frac{[4\text{Mn-bpy}][(\text{4Mn-bpy}) + (2\text{Mn-bpy})][\text{DMF}]}{[1\text{Mn-bpy}][\text{TEOA}]^2[\text{CO}_2]} \end{aligned} \quad (7)$$

The other Mn(i) complexes with the substituted bpy ligand also showed similar IR spectral changes during a similar experiment in the DMF–TEOA mixed solution (Fig. S7†). Therefore, these complexes also have the ability to capture CO_2 . The equilibrium constants are summarised in Table 1. It is noteworthy that the values of $K_2(\text{Mn-X}_2\text{bpy})$ are not drastically different from those of $K_1(\text{Mn-X}_2\text{bpy})$ of the three Mn complexes. The CO_2 insertion between the Mn–O bond might be a concerted reaction between the nucleophilic attack of the oxygen atom in the ligand to the carbon in CO_2 and the electrophilic attack of the central metal to the oxygen atom in CO_2 (Scheme 2).^{22,31,47} Since a higher electronic density of the central metal should induce acceleration of the former process while obstructing the latter one, these conflicting effects might cancel each other out.

All of the three 2Re-X₂bpy complexes also efficiently captured CO_2 even from gases containing low concentrations of CO_2 (eqn (5)). The equilibrium constants for $K_2(\text{Re-X}_2\text{bpy})$ are summarised in Table 2. $K_2(\text{Re-Br}_2\text{bpy})$ was the largest of the three Re(i) complexes, while the difference between $K_2(\text{Re-bpy})$ and $K_2(\text{Re-(MeO)}_2\text{bpy})$ was small.

Comparison of the CO_2 -capturing abilities of the Mn(i), Re(i) and W(0) complexes

As described in the previous section, both series of the Mn(i) and Re(i) complexes have high CO_2 -capturing abilities (Scheme 3). The CO_2 insertion reactions into 2Mn-X₂bpy were more favourable than those into 2Re-X₂bpy, equilibrium constants of which are defined as $K_2(\text{M-X}_2\text{bpy})$ ($\text{M} = \text{Mn}$ and Re) (Process 2). However, the CO_2 -capturing ability of 1Mn-X₂bpy in the presence of TEOA

Table 1 Equilibrium constants of the Mn complexes

Complex				
Metal	X	$K_1/10^{-3}$	$K_2/10^3 \text{ M}^{-1}$	K_3/M^{-1}
Mn(i)	H	0.22 ± 0.03	61 ± 12	14 ± 1
	Br	0.64 ± 0.03	42 ± 8	27 ± 4
	MeO	0.12 ± 0.01	84 ± 15	10 ± 1



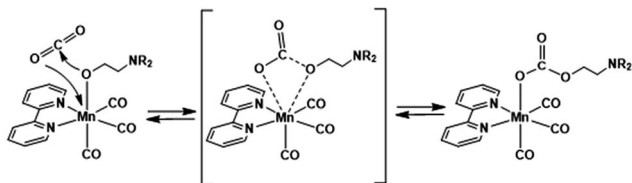
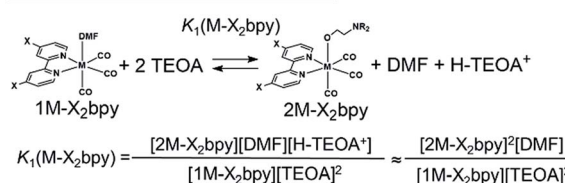
Scheme 2 Possible mechanism of CO_2 insertion into the M–O bond.

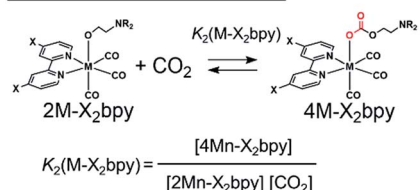
Table 2 Equilibrium constants of the Re complexes

Complex		$K_1/10^{-3}$	$K_2/10^3 \text{ M}^{-1}$	K_3/M^{-1}
Metal	X			
Re(i)	H	71 ± 1	1.2 ± 0.2	88 ± 13
	Br	128 ± 8	1.4 ± 0.1	179 ± 21
	MeO	30 ± 2	2.6 ± 0.1	79 ± 10

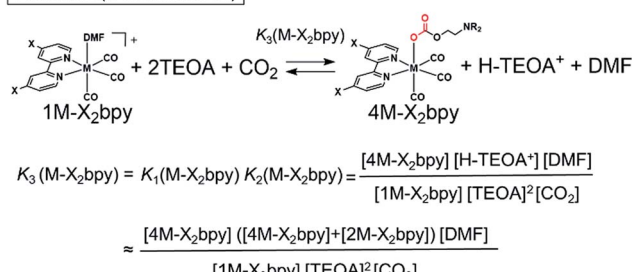
Process 1 (Ligand substitution reaction)



Process 2 (CO2 capture reaction)



Process 3 (Overall reaction)



Scheme 3 Reactions and the corresponding equilibrium constants for each step.

was lower than that of **1Re-X₂bpy**, and the equilibrium constants are defined as $K_3(\mathbf{M-X}_2\mathbf{bpy})$ (Process 3). This is because the formation of the TEOA adducts (**2Mn-X₂bpy** and **2Re-X₂bpy**), *i.e.*, Process 1, is much more favourable in the case of the Re complexes, the equilibrium constants of which are $K_1(\mathbf{M-X}_2\mathbf{bpy})$.

1Re-Br₂bpy as the starting complex most efficiently captured CO_2 from gases containing low concentrations of CO_2 in DMF including 1.3 M TEOA where the volume ratio between DMF and TEOA is 5 : 1; bubbling air containing only 400 ppm of CO_2 (1.7

$\times 10^{-4} \text{ M}$ in solution) into the DMF–TEOA mixed solution containing **1Re-Br₂bpy** and **2Re-Br₂bpy** converted 31% of the Re complexes into the corresponding CO_2 adduct, *i.e.*, **4Re-Br₂bpy**. This conversion ratio increased by changing the solvent to DMSO. In a DMSO solution containing 1.3 M TEOA, **4Re-Br₂bpy** formed at a 47% ratio under air.

Since the W(0) complex with a structure similar to that of the Re(i) and Mn(i) complexes has been reported, we checked the ligand substitution and CO_2 -capturing ability of *fac*-W(bpy)(CO)₃(MeCN). This complex was synthesised by dissolving W(bpy)(CO)₄ into an MeCN solution, which was refluxed under an Ar atmosphere overnight. Evaporation of the solvent gave *fac*-W(bpy)(CO)₃(MeCN) as a brown solid containing a small amount of W(bpy)(CO)₄. Since *fac*-W(bpy)(CO)₃(MeCN) was air-sensitive and W(bpy)(CO)₄ did not affect the following experiments, we used this solid.||

The FT-IR spectrum of *fac*-W(bpy)(CO)₃(MeCN) in an MeCN solution showed carbonyl vibration bands at $\nu_{\text{CO}} = 1898$ and 1782 cm^{-1} (Fig. S8†), which are consistent with a previous report.⁴⁸ This complex was dissolved in a DMF solution, and a CO vibration band at $\nu_{\text{CO}} = 1887 \text{ cm}^{-1}$ attributable to *fac*-W(bpy)(CO)₃(DMF) was observed (Fig. S9†). The other ν_{CO} bands overlapped with the carbonyl vibrational band of the DMF solvent and small absorption bands at $\nu_{\text{CO}} = 2005$, 1875, and 1831 cm^{-1} were attributed to *fac*-W(bpy)(CO)₄, which had the same wavelength and strength as those observed in the MeCN solution (Fig. 6). Addition of TEOA into the DMF solution containing W(bpy)(CO)₃(DMF) did not affect the ν_{CO} band at all under an Ar atmosphere. In addition, the CO vibration of *fac*-W(bpy)(CO)₃(DMF) in the IR spectra did not change after bubbling CO_2 through this solution (Fig. 6). These results clearly indicate that *fac*-[W(bpy)(CO)₃(OCH₂CH₂NR₂)][–] did not form from *fac*-W(bpy)(CO)₃(DMF) even in the presence of 1.3 M TEOA, and the CO_2 -capturing reaction also did not proceed under these reaction conditions (refer the equation in Fig. 6).

Gibbs free energy change and DFT calculation

The Gibbs free energy (G_f) changes in Processes 1–3 were calculated by using the equilibrium constants (K_1 , K_2 , and K_3) and are summarised in Table 3 (values in parentheses).

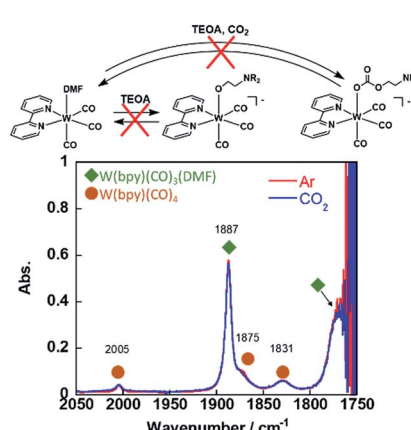
Fig. 6 IR spectra of W(bpy)(CO)₃ (DMF) in DMF–TEOA under Ar and CO_2 .

Table 3 Calculated and experimental^a changes in the Gibbs free energy (ΔG^0) of reactions 1–3 for the Mn(i), Re(i) and W(0) complexes

Metal	X	$\Delta G^0/\text{kJ mol}^{-1}$		
		Process 1	Process 2	Process 3
Mn(i)	H	10.1 (20.9)	−15.3 (−27.3)	−5.2 (−6.4)
	Br	8.9 (18.2)	−15.0 (−26.4)	−6.1 (−8.2)
	OMe	10.5 (22.4)	−10.3 (−28.1)	+0.2 (−5.7)
	H	−8.0 (6.55)	−2.6 (−17.6)	−10.6 (−11.1)
	Br	7.8 (5.09)	−25.6 (−18.0)	−17.8 (−12.9)
	OMe	11.2 (8.67)	−16.7 (−19.5)	−5.5 (−10.8)
W(0)	H	21.8	−9.0	12.8

^a Values in parentheses denote the experimental values calculated using $\Delta G^0 = -RT \ln K$ using $T = 298 \text{ K}$ and K_1 , K_2 and K_3 .

The observed abilities of the metal tricarbonyl complexes in the CO_2 -capturing reactions involving TEOA were examined based on the DFT calculations. Selected geometrical parameters calculated at the def2-SVP/PBE1PBE level including solvent effects are depicted in Table S2.† All of the Mn–N(bpy) and Mn–C(CO) bond lengths were calculated for **1Mn-bpy**, **2Mn-bpy** and **4Mn-bpy** with the singlet spin state and were in good agreement with those of the X-ray structure determined for *fac*-Mn(CO)₃(bpy)I,⁴⁹ supporting the accuracy of the DFT calculation. The geometrical optimisation of **1Re-bpy**, **2Re-bpy** and **4Re-bpy** also gave molecular structures with geometrical parameters similar to those of the X-ray structure of *fac*-Re(CO)₃(bpy)OC₅H₁₁.²³

The CO stretching vibrational frequencies of the tricarbonyl complexes were calculated for the DFT-optimised structures and were corrected using the reported scaling factor (Tables S3 and S5†).⁵⁰ While all of the calculated ν_{CO} values were slightly higher than the observed ones, the differences in ν_{CO} are almost constant for each series of the tricarbonyl complex: 31–50 cm^{-1} for Mn(i) complexes and 16–23 cm^{-1} for Re(i) complexes. The constant deviation in the calculated ν_{CO} supports the experimental identification of the species involved in the CO_2 -capturing reactions.

The changes in Gibbs free energy (ΔG^0) of each process for the Mn(i) and Re(i) complexes were then calculated based on the DFT calculations (Table 3). For the overall reaction (Process 3), these calculated ΔG^0 values are in good agreement with those obtained by the experiments with an error of 5 kJ mol^{-1} (~1 kcal mol^{−1}).

For CO_2 capture by the Mn complexes, the calculated ΔG^0 for reaction 1 is about 9–14 kJ mol^{-1} lower than the observed value, while those for Process 2 are 13–17 kJ mol^{-1} higher. This trend is also seen in the Re complexes even though the differences are smaller compared to those of the Mn complexes. These results are probably caused by an overestimation of the free energy of formation for the M–TEOA complexes (**2M-X₂bpy**). The TEOA moiety with three ethanol groups has several conformation

isomers. The geometrical optimisation of **2Mn-X₂bpy** and **4Mn-X₂bpy** gave somewhat compact structures due to intramolecular hydrogen bonding between the metal-coordinating O atom and the two remaining OH groups in the TEOA moiety.

The lengths of the hydrogen bonds in **4Mn-X₂bpy** are around 1.76–1.81 \AA . On the other hand, in the case of **2Mn-X₂bpy**, the hydrogen bonds between the anionic O atom, which is attached to the metal ion, and the OH groups are considerably short (1.50–1.59 \AA) (Fig. S10†). The same effects were observed in the Re complexes as well. Such strong intramolecular hydrogen bonding in **2M-X₂bpy** is one of the reasons for the overestimation of their stabilisation energies because, in the DMF–TEOA mixed solution, intermolecular hydrogen bonds with other TEOA molecules could break such a compact conformation and several other stable conformations would be formed. A more accurate prediction of ΔG^0 for the CO_2 insertion reaction therefore requires the evaluation of the TEOA conformational distribution including explicit interactions with other TEOA molecules. It should be noted that this uncertainty should not affect the ΔG^0 values of Process 3 because **2Mn-X₂bpy** and **2Re-X₂bpy** do not contribute to this process as shown in the equation for determining K_3 (Scheme 3). In other words, the errors based on the overestimation of the stabilisation energy of **2Mn-X₂bpy** and **2Re-X₂bpy** can be cancelled between Processes 1 and 2.

As described in the previous section, there are two possible equilibrium equations [eqn (1) and (3)] for the ligand substitution of DMF by TEOA. However, in solutions containing high concentration of TEOA (1.3 M), the reaction with one TEOA molecule acting as both a nucleophile and a base is considered unfavourable. The DFT calculation also supports this consideration because the observed ν_{CO} values (1902, 1918 and 2017 cm^{-1}) are close to those calculated for **2M-bpy** rather than for **2M-bpy-H⁺** (see Tables S3 and S4†). In addition, the calculated ΔG^0 corresponding to eqn (3) (14.5 kJ mol^{-1}) is higher than the ΔG^0 value for Process 1 (10.1 kJ mol^{-1}), which also indicates the favourability of eqn (1).

For the CO_2 -capturing reaction of the corresponding W(CO)₃(bpy)X species, the ΔG^0 values for Processes 1, 2, and 3 are calculated to be +21.8, −9.0, and +12.8 kJ mol^{-1} , respectively. The calculated large positive ΔG^0 value of Process 3 is consistent with the results showing that the W(0) complex was less reactive for the CO_2 -capturing reaction in the presence of TEOA compared to the Re(i) and Mn(i) complexes.

As shown for the three series of metal complexes consisting of different metal ions and different ligands, DFT was able to calculate the ΔG^0 values for the overall CO_2 -capturing reaction (Process 3) with good accuracy (~5 kJ mol^{-1}). We can use this method for estimating the CO_2 -capturing abilities of other metal complexes and to examine the mechanism of CO_2 -capturing reactions.

Experimental section

General procedures

FT-IR spectra were measured using a JASCO FT/IR-610 or 6600 spectrometer at 1 cm^{-1} resolution. ¹H NMR and ¹³C NMR spectra were measured in acetonitrile-*d*₃, DMF-*d*₇ or DMSO-*d*₆



using a JEOL ECA400-II at 400 and 100 MHz, respectively. Electrospray ionisation mass spectroscopy (ESI-MS) was performed using a Shimadzu LCMS-2010A system with acetonitrile as the mobile phase.

Materials

DMF was distilled under reduced pressure after pre-drying using activated molecular sieves of 4 Å and stored under Ar in a glove box. TEOA was distilled under reduced pressure and stored under Ar in a glove box. DMSO was distilled under reduced pressure after pre-drying overnight with CaH_2 under Ar. Acetonitrile was distilled three times over P_2O_5 and distilled again by CaH_2 before use. All other reagents of reagent-grade quality were used without further purification.

Calculation of equilibrium constants

Preparation procedures of the solutions for the measurements were performed in a glove box (UNICO, UN-650F) with a gas circulation dehydration device (DGE-05) under Ar (water content was less than 376 ppm). Concentrations of the complexes in solutions were obtained by the peak areas of ν_{CO} at the highest wavenumber (2000–2060 cm^{-1}) in the IR spectra. The peak areas attributed to each complex were obtained by curve-fitting using a linear combination of the Gaussian and the Lorentzian functions.^{18,19}

Ligand substitution reaction

The Mn(i) and W(0) diimine tricarbonyl acetonitrile complexes were dissolved in DMF solutions containing different concentrations of TEOA. The solutions were kept at room temperature in the dark for several hours and then their IR spectra were measured. In the case of the Re(i) complexes, the complexes with an acetonitrile ligand were dissolved in DMF to avoid the formation of **3Re-X₂bpy**. The solutions were kept at room temperature in the dark for several hours (>3 h), when all of the complexes were converted into **1Re-X₂bpy**, and then TEOA was added to these solutions. After keeping the solutions at room temperature in the dark for 2 h, the IR spectra of the equilibrium mixtures were recorded.

CO_2 -capturing reactions

Various amounts (0.020–0.025 mL) of a CO_2 -saturated DMF solution (the concentration of CO_2 is 0.20 M)^{18,19} were added to DMF solutions (1.8 mL) containing TEOA (1.3 M) and the equilibrium mixture of the metal complexes in a shielded sample tube by using a micro-syringe in a glove box. After the solutions were kept at room temperature for several hours, the IR spectra were measured.

Synthesis

fac-Re(X₂bpy)(CO)₃Br was synthesised according to a reported method.^{1,2} *fac*-Mn(X₂bpy)(CO)₃Br was synthesised according to a reported method with a small difference indicated as follows.¹⁵ All procedures for the synthesis of the Mn(i) complexes were performed in a dark room with red light. W(bpy)(CO)₄ and

fac-W(bpy)(CO)₃(MeCN) were synthesised according to a reported method.^{51,52}

fac-[Mn(bpy)(CO)₃(MeCN)][PF₆]. *fac*-Mn(bpy)(CO)₃Br (1.0 g, 2.7 mmol) and AgPF₆ (0.69 g, 2.7 mmol) were dissolved in 350 mL of Ar-saturated acetonitrile and this solution was heated at 40 °C for 1 h. After cooling to room temperature, the white precipitate of AgBr was removed by filtration with a Celite phase, and the solvent was evaporated. A yellow residue was dissolved in a small amount of CH₂Cl₂. *n*-Hexane was added to this solution to yield the target compound as a yellow precipitate, which was filtered and washed with a small amount of ether. Yield: 1.2 g (96%). ¹H NMR (400 MHz, chloroform-*d*₁, ppm): δ = 9.04 (d, 2H, *J* = 5.2 Hz, bpy-6,6'), 8.41 (d, 2H, *J* = 7.6 Hz, bpy-3,3'), 8.22 (dd, 2H, *J* = 7.6, 8.0 Hz bpy-4,4'), 7.66 (dd, 2H, *J* = 8.0, 5.2 Hz, bpy-5,5'), 2.10 (s, 3H, NC-CH₃). FT-IR (MeCN): ν (CO)/cm⁻¹, 2028, 1938, 1923. Elemental anal. calcd (%) for C₁₅H₁₁MnN₃O₃PF₆: C, 37.44; H, 2.30; N, 8.73. Found: C, 37.56; H, 2.21; N, 8.83.

The following Mn complexes were synthesised by a similar method to that of [Mn(bpy)(CO)₃(MeCN)][PF₆] except for using the corresponding Br complexes as the starting complexes.

fac-[Mn(4,4'-dibromo-2,2-bipyridine)(CO)₃(MeCN)][PF₆]. Yield: 0.45 g (95%). ¹H NMR (400 MHz, chloroform-*d*₁, ppm): δ = 8.83 (d, 2H, *J* = 6.8 Hz, bpy-6,6'), 8.42 (d, 2H, *J* = 2.4 Hz, bpy-3,3'), 7.82 (dd, 2H, *J* = 2.4, 6.8 Hz, bpy-5,5'), 2.16 (s, 3H, NC-CH₃, H). FT-IR (MeCN): ν (CO)/cm⁻¹, 2051, 1963. Elemental anal. calcd (%) for C₁₅H₉Br₂MnN₃O₃PF₆: C, 28.20; H, 1.42; N, 6.58. Found: C, 28.50; H, 1.28; N, 6.69.

fac-[Mn(4,4'-methoxy-2,2-bipyridine)(CO)₃(MeCN)][PF₆]. Yield: 0.26 g (75%). ¹H NMR (400 MHz, chloroform-*d*₁, ppm): δ = 8.72 (d, 2H, *J* = 6.4 Hz, bpy-6,6'), 7.81 (d, 2H, *J* = 2.6 Hz, bpy-3,3'), 7.82 (dd, 2H, *J* = 2.6, 6.4 Hz bpy-5,5'), 4.11 (s, 6H, -OCH₃) 2.16 (s, 3H, NC-CH₃). FT-IR (MeCN): ν (CO)/cm⁻¹, 2047, 1953. Elemental anal. calcd (%) for C₁₇H₁₅MnN₃O₅PF₆: C, 37.73; H, 2.79; N, 7.76. Found: C, 37.71; H, 2.72; N, 7.75.

fac-[Re(4,4'-dibromo-2,2-bipyridine)(CO)₃(MeCN)][PF₆]. Yield: 0.44 g (63%). ¹H NMR (400 MHz, acetonitrile-*d*₃, ppm): δ = 8.81 (d, 2H, *J* = 6.0 Hz, bpy-6,6'), 8.72 (d, 2H, *J* = 2.0 Hz, bpy-3,3'), 7.92 (dd, 2H, *J* = 2.0, 6.0 Hz, bpy-5,5'), 2.06 (s, 3H, NC-CH₃). FT-IR (MeCN): ν (CO)/cm⁻¹, 2042, 1941. Elemental anal. calcd (%) for C₁₅H₉Br₂ReN₃O₃PF₆: C, 23.39; H, 1.18; N, 5.46. Found: C, 23.56; H, 1.10; N, 5.62.

fac-[Re(4,4'-methoxy-2,2-bipyridine)(CO)₃(MeCN)][PF₆]. Yield: 0.44 g (62%). ¹H NMR (400 MHz, acetonitrile-*d*₃, ppm): δ = 8.76 (d, 2H, *J* = 6.0 Hz, bpy-6,6'), 7.92 (d, 2H, *J* = 2.0 Hz, bpy-3,3'), 7.19 (dd, 2H, *J* = 2.0, 6.0 Hz, bpy-5,5'), 4.03 (s, 6H, -OCH₃), 2.06 (s, 3H, NC-CH₃). FT-IR (MeCN): ν (CO)/cm⁻¹, 2038, 1932. Elemental anal. calcd (%) for C₁₇H₁₅ReN₃O₅PF₆: C, 30.36; H, 2.25; N, 6.25. Found: C, 30.85; H, 2.24; N, 6.43.

DFT calculations of changes in Gibbs free energy (ΔG^0)

The geometry optimisations of chemical species involved in CO_2 -capturing were carried out using a hybrid density functional with 25% exchange and a 75% Perdew, Burke, and Ernzerhof correlation functional (PBE1PBE)⁵³ using a smaller def2-SVP basis set with an effective core potential for Re and Br



atoms. The solvent DMF was modelled as a dielectric continuum using a polarisable continuum model.⁵⁴ The electronic energies were then obtained as the SCF energy of a single-point calculation on the optimised geometries using a larger basis set of def2-TZVP. The solvent effect of DMF was considered using the SMD method, a parametrised SCRF-based solvation model developed to predict the free energy of solvation.⁵⁵ The thermal correction terms to evaluate the standard Gibbs energy of formation (G_f) were computed by vibrational frequency analysis of the stationary structures using the same calculation level as for the geometry optimisations. An appropriate scaling factor of 0.9817 was used for the computed zero-point energy.⁵⁶ Changes in the Gibbs free energy (ΔG^0) were calculated as the difference in G_f between the reactants and the products. For the ΔG^0 values corresponding to K_2 and K_3 with the unit of M^{-1} , the calculated G_f values were corrected by -7.9 kJ mol^{-1} for the change in the reference states from 1 bar to 1 M.⁵⁶ All DFT calculations were executed using Gaussian 16 packages.⁵⁷

Conclusions

We found that the CO_2 -capturing reactions of Mn(i) diimine tricarbonyl complexes with a deprotonated TEOA ligand were similar to those of the corresponding Re(i) complexes. The equilibrium constants of both the Mn(i) and Re(i) diimine complexes for the ligand substitution (Process 1) and for CO_2 capture (Process 2) in DMF-TEOA solutions were determined. From the DFT calculations, in addition to these equilibrium constants, we systematically and quantitatively clarified the effects of both the metal and the substituents on the bpy ligand. This kind of metal affected both Processes 1 and 2. On the other hand, ligand substituents had a greater influence on Process 1 than Process 2. The DFT calculation can be applied to estimate the ΔG^0 of the total reaction containing both the ligand substitution and CO_2 capture (Process 3), and the ΔG^0 values were in good agreement with those calculated from the experimental data. The CO_2 -capturing reaction of $\text{W}(\text{bpy})(\text{CO})_3(\text{DMF})$ in the TEOA-DMF solution did not proceed at all because of the large ΔG^0 value for Process 3. These calculation approaches can give a good approximation to judge whether the total CO_2 -capturing phenomenon (Process 3) proceeds or not with various metal complexes.

Conflicts of interest

There are no conflicts of interest to declare.

Acknowledgements

This work was supported by JST CREST Grant number JPMJCR13L1. This work was also partially supported by JSPS KAKENHI Grant number 17H06440 in Scientific Research on Innovative Areas 'Innovations for Light-Energy Conversion (I4LEC)'.

Notes and references

† As shown in Table S1, a similar discussion can be done by using K'_1 instead of K_1 .

‡ Unfortunately, we could not use the step-by-step substitution synthesis method in the case of the Mn complexes because dissolving $\text{fac-}[\text{Mn}(\text{bpy})(\text{CO})_3(\text{MeCN})]^+$ into DMF gave not only **1Mn-bpy** but also a minor product which we have not been able to identify. As described above, therefore, we dissolved the Mn complexes directly into the DMF-TEOA mixed solution.

¶ In this experiment, we observed other small bands at 2019 cm^{-1} , peaks of which appeared and gradually increased after the addition of TEOA. This species was probably attributed to the formato complex $\text{Re}(\text{bpy})(\text{CO})_3(\text{OCHO})$, the formate ligand of which was probably supplied from DMF. This decomposition of DMF under basic conditions with TEOA and H_2O was reported by Vos and his coworkers.⁵⁸ It was also reported that this reaction is suppressed under more acidic conditions such as under a CO_2 atmosphere. We used well dehydrated TEOA and DMF and minimized the time for measuring the IR spectra of the equilibrated mixtures under an Ar atmosphere after addition of TEOA (typically 120 min) for minimizing formation yields. The formation of the formato complex was less than 3% in all the Re complexes. In the case of Mn(i) complexes, this formation of the formato complex was very slow.

|| $\text{W}(\text{bpy})(\text{CO})_3(\text{MeCN})$ was unstable in air probably because of oxidation of the metal centre and decarbonylation. Therefore, $\text{W}(\text{bpy})(\text{CO})_3(\text{MeCN})$ was used without any purification after the synthesis.

- 1 J. Hawecker, J.-M. Lehn and R. Ziessel, *J. Chem. Soc., Chem. Commun.*, 1983, 536–538.
- 2 M. Bourrez, F. Molton, S. Chardon-noblat and A. Deronzier, *Angew. Chem., Int. Ed.*, 2011, **50**, 9903–9906.
- 3 H. Ishida, T. Terada, K. Tanaka and T. Tanaka, *Inorg. Chem.*, 1990, **29**, 905–911.
- 4 S. Sato, T. Morikawa, T. Kajino and O. Ishitani, *Angew. Chem., Int. Ed.*, 2013, **52**, 988–992.
- 5 V. S. Thoi, N. Kornienko, C. G. Margarit, P. Yang and C. J. Chang, *J. Am. Chem. Soc.*, 2013, **135**, 14413–14424.
- 6 D. Hong, Y. Tsukakoshi, H. Kotani, T. Ishizuka and T. Kojima, *J. Am. Chem. Soc.*, 2017, **139**, 6538–6541.
- 7 L. Chen, Z. Guo, X. G. Wei, C. Gallenkamp, J. Bonin, E. Anxolabéhère-Mallart, K. C. Lau, T. C. Lau and M. Robert, *J. Am. Chem. Soc.*, 2015, **137**, 10918–10921.
- 8 H. Takeda, K. Ohashi, A. Sekine and O. Ishitani, *J. Am. Chem. Soc.*, 2016, **138**, 4354–4357.
- 9 A. Rosas-Hernández, P. G. Alsabeh, E. Barsch, H. Junge, R. Ludwig and M. Beller, *Chem. Commun.*, 2016, **52**, 8393–8396.
- 10 Z. Guo, S. Cheng, C. Cometto, E. Anxolabéhère-Mallart, S.-M. Ng, C.-C. Ko, G. Liu, L. Chen, M. Robert and T.-C. Lau, *J. Am. Chem. Soc.*, 2016, **138**, 9413–9416.
- 11 H. Rao, L. C. Schmidt, J. Bonin and M. Robert, *Nature*, 2017, **548**, 74–77.
- 12 J. Shen, R. Kortlever, R. Kas, Y. Y. Birdja, O. Diaz-Morales, Y. Kwon, I. Ledezma-Yanez, K. J. P. Schouten, G. Mul and M. T. M. Koper, *Nat. Commun.*, 2015, **6**, 1–8.
- 13 T. Ouyang, H.-H. Huang, J.-W. Wang, D.-C. Zhong and T.-B. Lu, *Angew. Chem., Int. Ed.*, 2017, **56**, 738–743.
- 14 J. Hawecker, J.-M. Lehn and R. Ziessel, *J. Chem. Soc., Chem. Commun.*, 1984, **6**, 328–330.
- 15 H. Takeda, H. Koizumi, K. Okamoto and O. Ishitani, *Chem. Commun.*, 2014, **50**, 1491–1493.
- 16 M. D. Sampson, A. D. Nguyen, K. A. Grice, C. E. Moore, A. L. Rheingold and C. P. Kubiak, *J. Am. Chem. Soc.*, 2014, **136**, 5460–5471.



17 J. Agarwal, T. W. Shaw, H. F. Schaefer and A. B. Bocarsly, *Inorg. Chem.*, 2015, **54**, 5285–5294.

18 T. Morimoto, T. Nakajima, S. Sawa, R. Nakanishi, D. Imori and O. Ishitani, *J. Am. Chem. Soc.*, 2013, **135**, 16825–16828.

19 T. Nakajima, Y. Tamaki, K. Ueno, E. Kato, T. Nishikawa, K. Ohkubo, Y. Yamazaki, T. Morimoto and O. Ishitani, *J. Am. Chem. Soc.*, 2016, **138**, 13818–13821.

20 S. K. Mandal, D. M. Ho and M. Orchin, *Organometallics*, 1993, **12**, 1714–1719.

21 D. J. Darensbourg, W. Z. Lee, A. L. Phelps and E. Guidry, *Organometallics*, 2003, **22**, 5585–5588.

22 R. D. Simpson and R. G. Bergman, *Organometallics*, 1992, **11**, 4306–4315.

23 M. K. Mbagu, D. N. Kebulu, A. Winstead, S. K. Pramanik, H. N. Banerjee, M. O. Iwunze, J. M. Wachira, G. E. Greco, G. K. Haynes, A. Sehmer, F. H. Sarkar, D. M. Ho, R. D. Pike and S. K. Mandal, *Inorg. Chem. Commun.*, 2012, **21**, 35–38.

24 T. Tsuda and T. Saegusa, *Inorg. Chem.*, 1972, **11**, 2561–2563.

25 S. M. Kupchan and C. Kim, *J. Am. Chem. Soc.*, 1975, **97**, 5625–5627.

26 A. Immirizi and A. Musco, *Inorg. Chim. Acta*, 1977, **22**, 35–36.

27 T. Yamamoto, M. Kubota and A. Yamamoto, *Bull. Chem. Soc. Jpn.*, 1980, **53**, 680–685.

28 L. J. Newman and R. G. Bergman, *J. Am. Chem. Soc.*, 1985, **107**, 5314–5315.

29 M. Kato and T. Ito, *Inorg. Chem.*, 1985, **24**, 509–514.

30 D. J. Darensbourg, K. M. Sanchez, J. H. Reibenspies and A. L. Rheingold, *J. Am. Chem. Soc.*, 1989, **111**, 7094–7103.

31 D. J. Darensbourg, B. L. Mueller, C. J. Bischoff, S. S. Chojnacki and J. H. Reibenspies, *Inorg. Chem.*, 1991, **30**, 2418–2424.

32 B. Buffin, A. Arif and T. Richmond, *J. Chem. Soc., Chem. Commun.*, 1993, **18**, 1432–1434.

33 M. Ruf and H. Vahrenkamp, *Inorg. Chem.*, 1996, **35**, 6571–6578.

34 M. Aresta, A. Dibenedetto and C. Pastore, *Inorg. Chem.*, 2003, **42**, 3256–3261.

35 D. R. Moore, M. Cheng, E. B. Lobkovsky and G. W. Coates, *J. Am. Chem. Soc.*, 2003, **125**, 11911–11924.

36 M. M. Ibrahim, K. Ichikawa and M. Shiro, *Inorg. Chem. Commun.*, 2003, **6**, 1030–1034.

37 O. Tardif, D. Hashizume and Z. Hou, *J. Am. Chem. Soc.*, 2004, **126**, 8080–8081.

38 H. Brombacher and H. Vahrenkamp, *Inorg. Chem.*, 2004, **43**, 6042–6049.

39 D. Cui, M. Nishiura, O. Tardif and Z. Hou, *Organometallics*, 2008, **27**, 2428–2435.

40 E. C. Y. Tam, N. C. Johnstone, L. Ferro, P. B. Hitchcock and J. R. Fulton, *Inorg. Chem.*, 2009, **48**, 8971–8976.

41 L. A. M. Steele, T. J. Boyle, R. A. Kemp and C. Moore, *Polyhedron*, 2012, **42**, 258–264.

42 A. Arunachalampillai, N. Loganathan and O. F. Wendt, *Polyhedron*, 2012, **32**, 24–29.

43 B. J. Truscott, D. J. Nelson, A. M. Z. Slawin and S. P. Nolan, *Chem. Commun.*, 2014, **50**, 286–288.

44 Y. Arikawa, T. Nakamura, S. Ogushi, K. Eguchi and K. Umakoshi, *Dalton Trans.*, 2015, **44**, 5303–5305.

45 F. Parrino, C. Deiana, M. R. Chierotti, G. Martra and L. Palmisano, *J. CO₂ Util.*, 2016, **13**, 90–94.

46 J.-C. Choi, H.-Y. Yuan, N. Fukaya, S. Onozawa, Q. Zhang, S. J. Choi and H. Yasuda, *Chem.-Asian J.*, 2017, **12**, 1297–1300.

47 S. V. C. Vummaleti, G. Talarico, S. P. Nolan, L. Cavallo and A. Poater, *Eur. J. Inorg. Chem.*, 2015, **28**, 4653–4657.

48 T. E. Dorsett and R. A. Walton, *J. Chem. Soc., Dalton Trans.*, 1976, 347–350.

49 G. J. Stor, D. J. Stufkens, P. Vernooij, E. J. Baerends, J. Fraanje and K. Goubitz, *Inorg. Chem.*, 1995, **34**, 1588–1594.

50 M. K. Kesharwani, B. Brauer and J. M. L. Martin, *J. Phys. Chem. A*, 2015, **119**, 1701–1714.

51 T. S. A. Hor and S.-M. Chee, *J. Organomet. Chem.*, 1987, **331**, 23–28.

52 Y. Yamaguchi, H. Nakazawa, T. Itoh and K. Miyoshi, *Bull. Chem. Soc. Jpn.*, 1996, **69**, 983–998.

53 C. Adamo and V. Barone, *J. Chem. Phys.*, 1999, **110**, 6158–6169.

54 J. Tomasi, B. Mennucci and E. Cancès, *J. Mol. Struct.: THEOCHEM*, 1999, **464**, 211–226.

55 A. V. Marenich, C. J. Cramer and D. G. Truhlar, *J. Phys. Chem. B*, 2009, **113**, 6378–6396.

56 J. Keith and E. A. Carter, *J. Chem. Theory Comput.*, 2012, **8**, 3187–3206.

57 M. J. Frisch, G. W. Trucks, H. B. Schlegel, G. E. Scuseria, M. A. Robb, J. R. Cheeseman, G. Scalmani, V. Barone, G. A. Petersson, H. Nakatsuji, X. Li, M. Caricato, A. V. Marenich, J. Bloino, B. G. Janesko, R. Gomperts, B. Mennucci, H. P. Hratchian, J. V. Ortiz, A. F. Izmaylov, J. L. Sonnenberg, D. Williams-Young, F. Ding, F. Lipparini, F. Egidi, J. Goings, B. Peng, A. Petrone, T. Henderson, D. Ranasinghe, V. G. Zakrzewski, J. Gao, N. Rega, G. Zheng, W. Liang, M. Hada, M. Ehara, K. Toyota, R. Fukuda, J. Hasegawa, M. Ishida, T. Nakajima, Y. Honda, O. Kitao, H. Nakai, T. Vreven, K. Throssell, J. A. Montgomery Jr, J. E. Peralta, F. Ogliaro, M. J. Bearpark, J. J. Heyd, E. N. Brothers, K. N. Kudin, V. N. Staroverov, T. A. Keith, R. Kobayashi, J. Normand, K. Raghavachari, A. P. Rendell, J. C. Burant, S. S. Iyengar, J. Tomasi, M. Cossi, J. M. Millam, M. Klene, C. Adamo, R. Cammi, J. W. Ochterski, R. L. Martin, K. Morokuma, O. Farkas, J. B. Foresman, and D. J. Fox, *Gaussian 16, Revision B.01*, Gaussian, Inc., Wallingford CT, 2016.

58 A. Paul, D. Connolly, M. Schulz, M. T. Pryce and J. G. Vos, *Inorg. Chem.*, 2012, **51**, 1977–1979.

